CHAPTER 3

RESULTS AND DISCUSSION

3.1 Flow injection system with in-valve ion exchanger mini-column for preconcentration of cadmium, copper, lead and zinc determination coupled to flame atomic absorption spectrometer

3.1.1 Optimization of FI system with in-valve column

3.1.1.1 Effect of elution flow rate on the elution step

Using the FI system for the previous FI-FAAS set-up (Figure 2.2), the effect of elution flow rate was studied in the off-line mode by taking off the line at the point of connecting to the sample loop of the IC valve. A standard Cu solution was loaded on the mini-column. In the elution process, 2.0 M HNO_3 was used to elute the analyte, Cu, from the mini-column, and the eluent flow rate was varied: 1, 2, 3, 4, 5 and 6 ml min^{-1}. Fractions of eluent were collected from the off-line FI system and the resulting fractions were analysed by FAAS. It was found that no significant absorbance change occurred at the studied flow rates (Table 3.1 and Figure 3.1). A 5 ml min^{-1} elution flow rate was suitable for the further work due to the good reproducibility in absorbance signal (1.5% RSD), and the flow rate was higher than the uptake rate of the nebulizer (takeup rate 4.8 ml min^{-1}). The flow rate

transportation into the nebulizer should match, or least be close to, the free uptake flow rate of the pneumatic nebulizer [81].

Table 3.1 Effect of eluent flow rate

Flow rate of eluent ($ml\ min^{-1}$)	Average absorbance of Cu (n=3)	%RSD
1	0.065	3.2
2	0.062	4.1
3	0.062	2.5
4	0.067	3.9
5	0.067	1.5
6	0.062	1.6

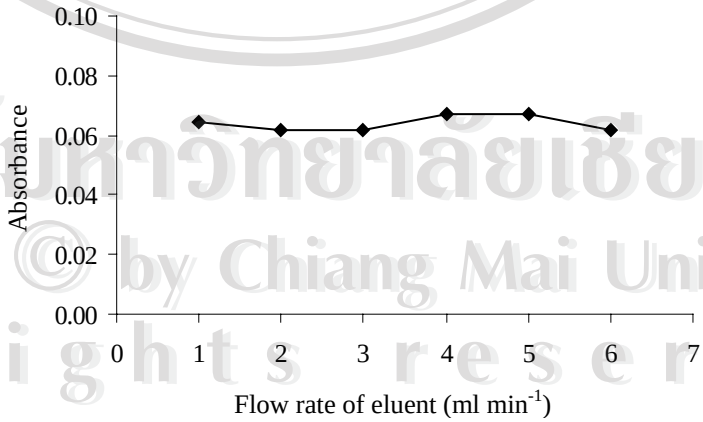

Figure 3.1 Effect of eluent flow rate

3.1.1.2 Effect of loading flow rate on the preconcentration step

Using the manifold described in 2.4.1 and in Figure 2.2, the effect of sample loading flow rate on the preconcentration of cations was checked. A series of standards of each cation (Cd, Cu, Pb and Zn) was prepared and loaded onto the Chelex-100 mini-column with flow rates of 2, 3 and 4 ml min^{-1}. Loading time was also varied to result in the same amount in micrograms by considering: μg=(c μg ml^{-1}) x (q ml min^{-1}) x (t min) where c, q and t are concentration, flow rate and loading time, respectively. It was found that the studied loading flow rates resulted in no significant difference in peak heights for all the cations studied (Figure 3.2). And the signal (peak height) of Zn was linear after 1.0 μg of Zn (Figure 3.2d), due to the limitation of Beer's law on the absorption in FAAS. Considering the same μg of cation from flow rates of 2, 3 and 4 ml min^{-1}, the flow rate of 2 ml min^{-1} required longer loading time than the others, and the flow rate of 4 ml min^{-1} consumed more sample throughput. The flow rate of 3 ml min^{-1} was considered for sample loading. And ammonium acetate buffer at a flow rate 1.5 ml min^{-1} for the solution loaded on the mini-column was also considered.

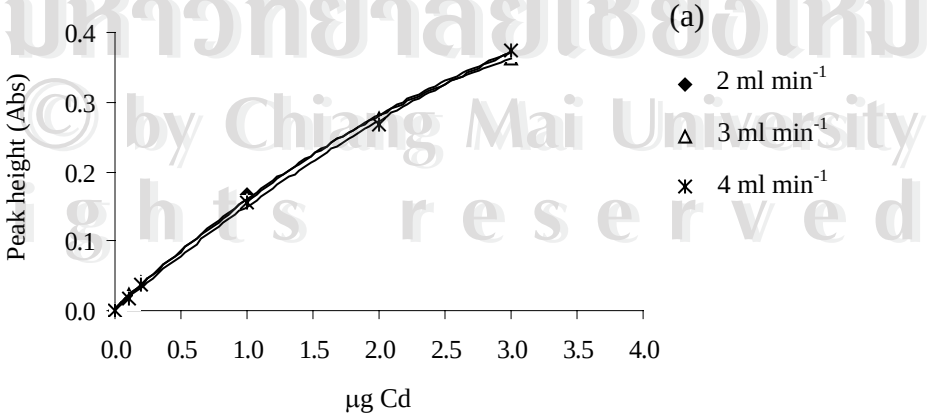

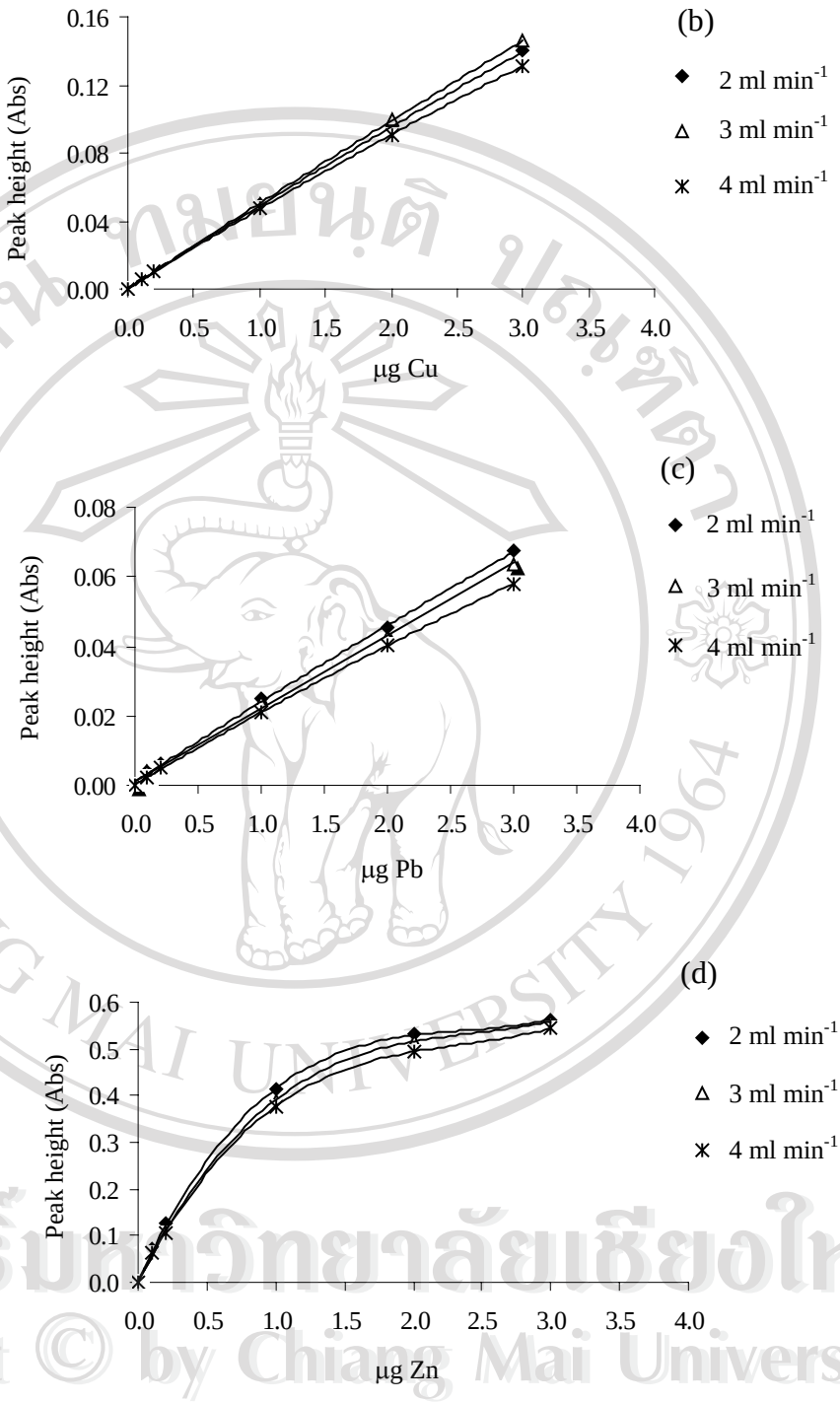

Figure 3.2 Effect of flow rate on the preconcentration step of (a) Cd, (b) Cu, (c) Pb and (d) Zn

3.1.1.3 Effect of ammonium acetate buffer concentration

The pH value of the solution in the mini-column is the most important parameter in the Chelex-100 resin because the resin contains weakly acidic functional groups, and the pH of a solution in the column may be affected by the resin itself and may change during the sorption processes if an external buffer system is not used [82]. An ammonium acetate buffer pH 5.4 was used to adjust the sample/standard solution during the sorption process. Various buffer concentrations (0.1, 0.5, 1.0, 1.5 and 2.0 M) of ammonium acetate buffer were studied. Each concentration of buffer solution was used to control the pH of standard cation solutions. A series of standard copper solutions (0.05, 0.10, 0.50, 1.00 and 1.50 μl ml^{-1} Cu) was chosen to check the effect of buffer concentration. The concentration of acetate buffer pH 5.4 was varied for studies of the ability of the buffer to control the pH of standard/sample solution in the adsorption process, by checking the signal of the cation. The loading flow rate was 3 ml min^{-1} and loading time was 40 seconds. The results are summarized in Table 3.2 and Figure 3.3. It was found that the concentration range of 0.5-2.0 M buffers yielded no significant difference on the slopes of calibrations, but a 0.1 M buffer gave distinctly lower signals. The higher concentration would increase viscosity of solutions and may then reduce nebulizer performance. The concentration of 1.0 M ammonium acetate buffer was chosen for this study.

Table 3.2 Effect of concentration of ammonium acetate buffer

Loading time (sec)	Loading flow rate (ml min^{-1})	µg ml^{-1} Cu	µg Cu	Peak height at different buffer concentration (Abs)				
				0.1 M	0.5 M	1.0 M	1.5 M	2.0 M
40	3	0.05	0.1	0.0058	0.0073	0.0065	0.0065	0.0063
		0.1	0.2	0.0109	0.0143	0.0143	0.0135	0.0133
		0.5	1.0	0.0500	0.0695	0.0643	0.0627	0.0627
		1.0	2.0	0.0992	0.1250	0.1190	0.1141	0.1121
		1.5	3.0	0.1460	0.1763	0.1731	0.1688	0.1677

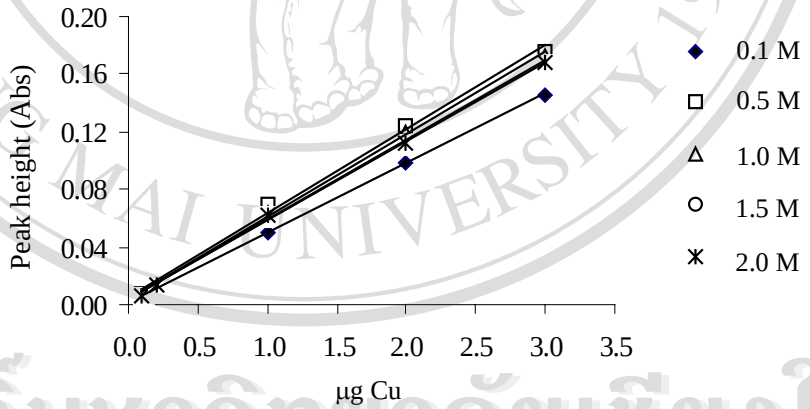

Figure 3.3 Effect of acetate buffer concentration on calibration graph of copper

3.1.1.4 pH of standard/sample solution in preconcentration step

The effect of the standard sample pH on the analyte retention was studied by varying the pH within the range of 1-4. A mixture of cations was adjusted to pH 1-4 with nitric acid and on-line mixed with 1.0 M ammonium acetate buffer prior to loading into the mini-column. It was found that no significant difference on the peak height was observed for the range 1-4. From results, the pH of water samples was 1.5 after acid preservation, and could be loaded on the column in the preconcentration step.

3.1.1.5 Counter ion form of Chelex-100 resin

The forms (hydrogen and ammonium) of Chelex-100 ion exchange resins were studied, and no significant difference was found, as the results summarized in Figure 3.4 show. The hydrogen form was chosen for further work due to no need for the process of conversion from H^+ to NH_4^+ form and due to the tendency of this resin to swell when converted from the hydrogen form to the ammonium form [54,83].

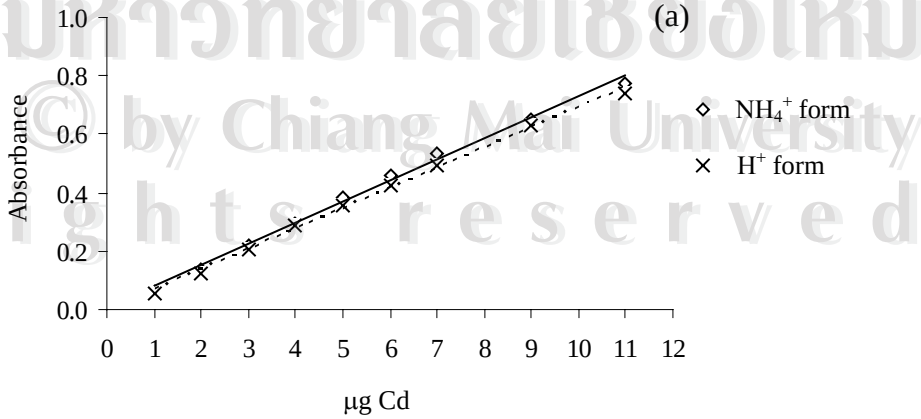

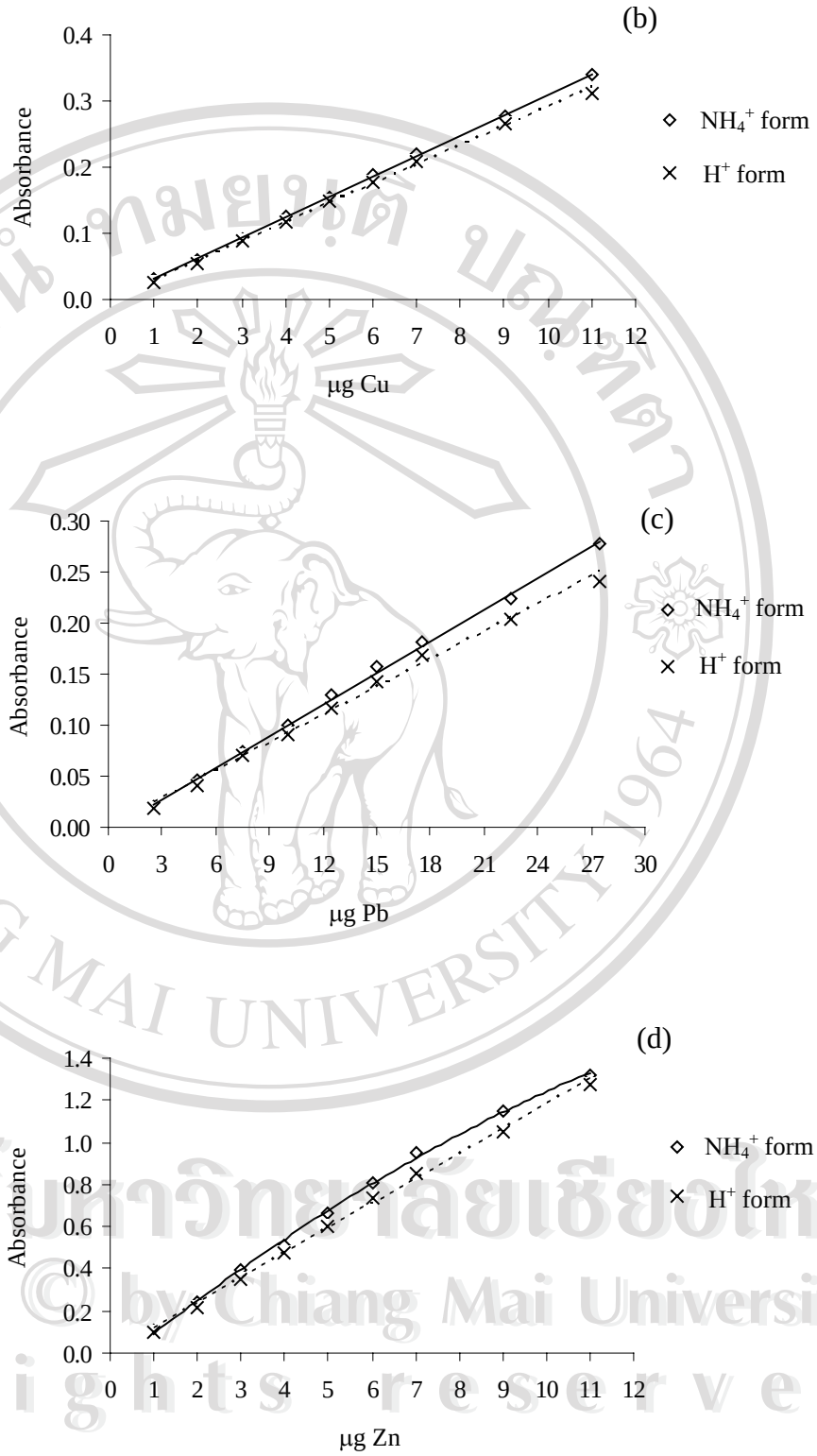

Figure 3.4 Comparisons of Chelex-100 resin in the forms of ammonium and hydrogen (a) Cd, (b) Cu, (c) Pb and (d) Zn

3.1.2 Calibration

3.1.2.1 Conventional calibration graph

Using the FI-FAAS manifold in Figure 2.2, conventional calibration graphs of cations were constructed by loading a series of mixtures of standards (0.01, 0.05, 0.10, 0.20, 0.40, 0.60 and 0.80 μg ml^{-1} Cd, 0.01, 0.05, 0.10, 0.30, 0.50, 0.70 and 1.00 μg ml^{-1} Cu, 0.05, 0.10, 0.50, 0.70, 1.00, 1.20 and 1.50 μg ml^{-1} Pb and 0.05, 0.10, 0.20, 0.40, 0.60, 0.80 and 1.00 μg ml^{-1} Zn) at a flow rate of 3 ml min^{-1} and loading time of 1 minute. The summary results of conventional calibration (Table 3.3) and the conventional calibration data and calibration graphs are represented in Tables 3.4-3.7 and Figures 3.5-3.8, respectively. The plot between series of concentrations of cation and peak height were found to be linear in the range 0.01-0.40 μg ml^{-1} for Cd, 0.01-1.00 μg ml^{-1} for Cu, 0.05-1.50 μg ml^{-1} for Pb and 0.05-0.20 μg ml^{-1} for Zn.

Table 3.3 Summary results of conventional calibration of cations

Cation	Equation	Correlation coefficient	Linear range (μg ml^{-1})
Cd	y=0.7493x+0.0150	0.9955	0.01-0.40
Cu	y=0.1606x+0.0035	0.9973	0.01-1.00
Pb	y=0.0427x+0.0038	0.9968	0.05-1.50
Zn	y=1.2821x+0.0253	0.9979	0.05-0.20

Table 3.4 Conventional calibration data of Cd using a loading flow rate 3 ml min^{-1} and loading time 1 minute

μg ml^{-1} Cd	Peak height (Abs)
0.01	0.0131
0.05	0.0511
0.10	0.1004
0.20	0.1700
0.40	0.3100
0.60	0.3979
0.80	0.4602

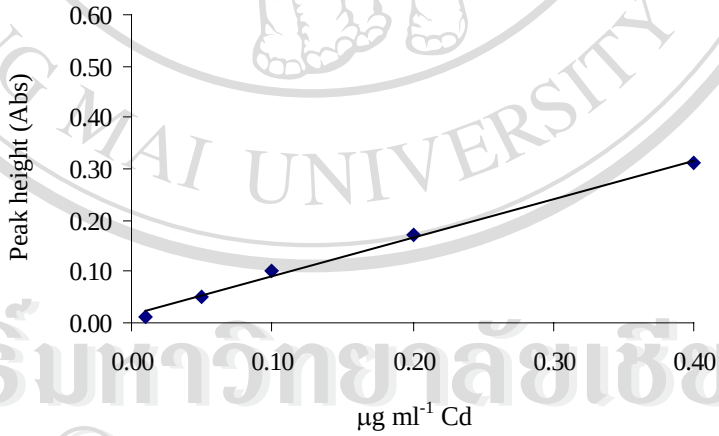

Figure 3.5 Conventional calibration graph of Cd

Table 3.5 Conventional calibration data of Cu using a loading flow rate 3 ml min^{-1} and loading time 1 minute

μg ml^{-1} Cu	Peak height (Abs)
0.01	0.0025
0.05	0.0098
0.10	0.0196
0.30	0.0352
0.50	0.0848
0.70	0.1200
1.00	0.1598

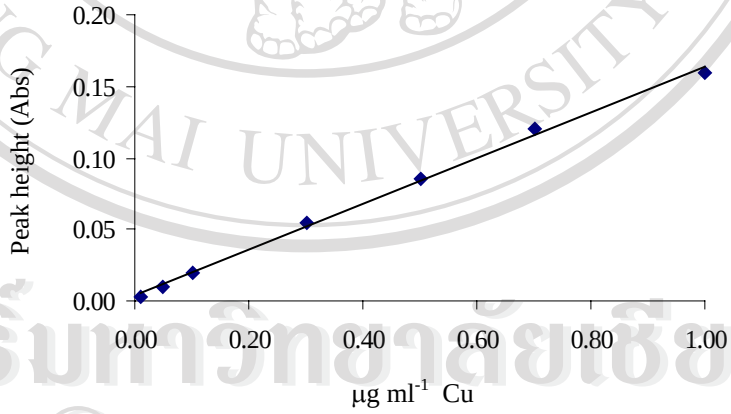

Figure 3.6 Conventional calibration graph of Cu

Table 3.6 Conventional calibration data of Pb using a loading flow rate 3 ml min^{-1} and loading time 1 minute

μg ml^{-1} Pb	Peak height (Abs)
0.05	0.0045
0.10	0.0076
0.50	0.0260
0.70	0.0350
1.00	0.0481
1.20	0.0550
1.50	0.0660

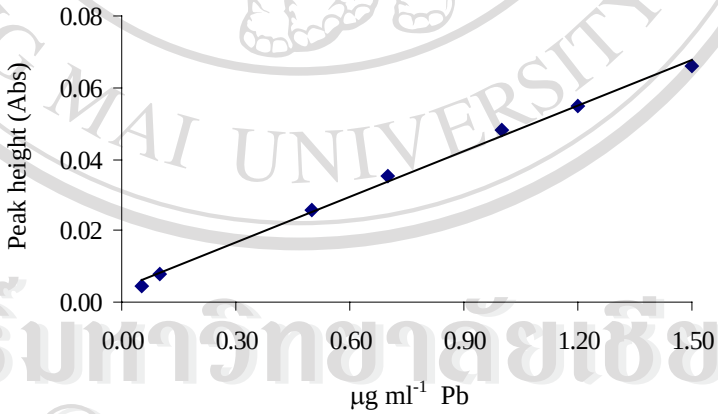

Figure 3.7 Conventional calibration graph of Pb

Table 3.7 Conventional calibration data of Zn using a loading flow rate 3 ml min^{-1} and loading time 1 minute

μg ml^{-1} Zn	Peak height (Abs)
0.05	0.0860
0.10	0.1585
0.20	0.2800
0.40	0.4200
0.60	0.4701
0.80	0.4670
1.00	0.4768

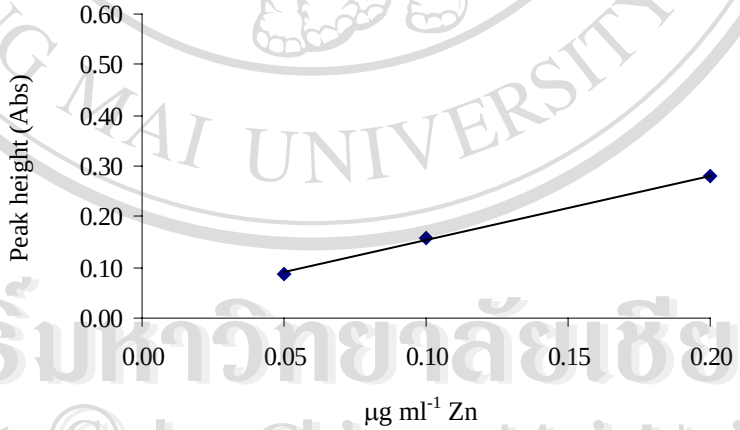

Figure 3.8 Conventional calibration graph of Zn

3.1.2.2 Single standard calibration graph

For the FI-FAAS with in-valve mini-column, single standard solutions of each of the cations were loaded on the mini-column with different loading times by using a loading flow rate of 3 ml min^{-1}. A single standard calibration was considered by using a plot of micrograms of cation loaded, calculated from the concentration of cation (μg ml^{-1}) of the standard solution, constantly loading flow rate (ml min^{-1}) and various loading times (min), versus peak height. The plots were found to be linear in the ranges 0.03-0.30 μg for Cd, 0.15-4.5 μg for Cu, 0.15-6.0 μg for Pb and 0.03-0.60 μg for Zn. In addition, a check was made that the single standard graph procedure can be used by comparing peak heights obtained from different standard concentrations with different loading times. It was found that peak heights were not changed within amounts of cations of 0.30 μg Cd, 4.5 μg Cu, 6.0 μg Pb and 0.60 μg Zn as shown in Tables 3.8-3.11 and Figures 3.9-3.12. The results were found that single standard solution of cations (Cd, Cu, Pb and Zn) can be use for single standard calibration in the limit range as above by changing loading time.

Table 3.8 Calibration data of Cd by fixing loading flow rate at 3 ml min^{-1}, various loading times at different concentrations

μg ml^{-1}Cd	Loading time (min)	μg Cd	Peak height (Abs)
0.01	1.0	0.03	0.0129
0.01	1.5	0.045	0.0172
0.005	4.0	0.06	0.0237
0.01	2.0	0.06	0.0201
0.01	2.0	0.06	0.0244
0.005	10	0.15	0.0452
0.01	5.0	0.15	0.0480
0.05	1.0	0.15	0.0542
0.05	1.5	0.225	0.0793
0.01	10	0.30	0.0824
0.05	2.0	0.30	0.0954
0.05	2.0	0.30	0.0854
0.10	1.0	0.30	0.0959
0.10	1.5	0.45	0.1317
0.10	2.0	0.60	0.1599

Table 3.8 Calibration data of Cd by fixing loading flow rate at 3 ml min^{-1}, various loading times at different concentrations (continued)

µg ml^{-1}Cd	Loading time (min)	µg Cd	Peak height (Abs)
0.5	1.0	1.5	0.3629
0.5	1.5	2.25	0.4462
0.5	2.0	3.0	0.5134
1.0	1.0	3.0	0.5020

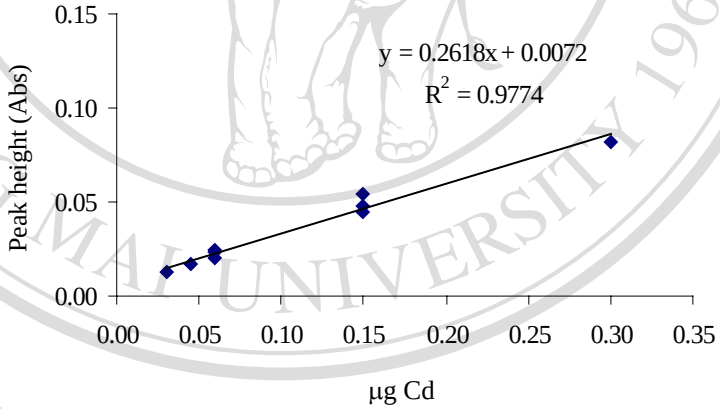

Figure 3.9 Calibration graph of Cd by various loading times at loading flow rate 3 ml min^{-1}

Table 3.9 Calibration data of Cu by fixing loading flow rate at 3 ml min^{-1}, various loading times at different concentrations

μg ml^{-1}Cu	Loading time (min)	μg Cu	Peak height (Abs)
0.01	1.0	0.03	0.0025
0.01	1.5	0.045	0.0033
0.01	2.0	0.06	0.0036
0.005	10	0.15	0.0089
0.05	1.0	0.15	0.0096
0.005	15	0.225	0.0124
0.05	1.5	0.225	0.0133
0.05	2.0	0.30	0.0163
0.10	1.0	0.30	0.0179
0.10	1.0	0.30	0.0196
0.10	1.5	0.45	0.0296
0.10	1.5	0.45	0.0252
0.10	2.0	0.60	0.0312
0.50	1.0	1.5	0.0848
0.50	1.5	2.25	0.1217
0.50	2.0	3.0	0.1514
1.0	1.0	3.0	0.1598
1.0	1.5	4.5	0.2348

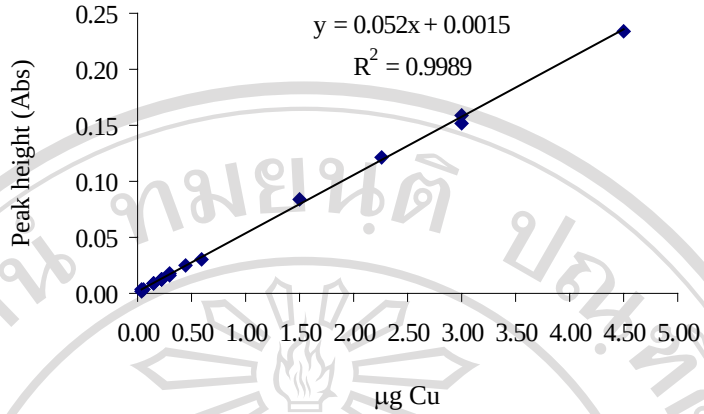

Figure 3.10 Calibration graph of Cu by various loading times at loading flow rate 3 ml min^{-1}

Table 3.10 Calibration data of Pb by fixing loading flow rate at 3 ml min^{-1}, various loading times at different concentrations

µg ml^{-1} Pb	Loading time (min)	µg Pb	Peak height (Abs)
0.005	10	0.15	0.0051
0.05	1.0	0.15	0.0040
0.05	1.0	0.15	0.0051
0.005	15	0.225	0.0059
0.05	1.5	0.225	0.0048
0.005	20	0.30	0.0067
0.05	2.0	0.30	0.0066

Table 3.10 Calibration data of Pb by fixing loading flow rate at 3 ml min^{-1}, various loading times at different concentrations (continued)

μg ml^{-1} Pb	Loading time (min)	μg Pb	Peak height (Abs)
0.10	1.0	0.30	0.0062
0.10	1.0	0.30	0.0072
0.10	1.5	0.45	0.0081
0.10	1.5	0.45	0.0097
0.10	2.0	0.60	0.0120
0.10	2.0	0.60	0.0092
0.50	1.0	1.5	0.0250
0.50	1.5	2.25	0.0353
0.50	2.0	3.0	0.0440
1.0	1.0	3.0	0.0476
1.0	1.5	4.5	0.0657
1.0	2.0	6.0	0.0814

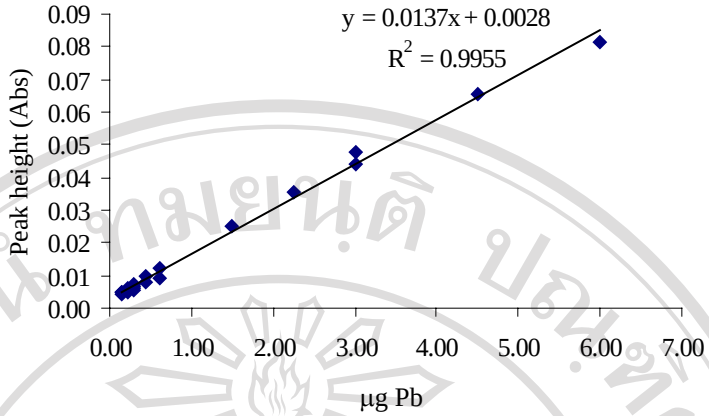

Figure 3.11 Calibration graph of Pb by various loading times at loading flow rate 3 ml min^{-1}

Table 3.11 Calibration data of Zn by fixing loading flow rate at 3 ml min^{-1}, various loading times at different concentrations

µg ml^{-1} Zn	Loading time (min)	µg Zn	Peak height (Abs)
0.01	1.0	0.03	0.0258
0.01	1.5	0.045	0.0416
0.01	2.0	0.06	0.0519
0.005	5.0	0.075	0.0645
0.005	10	0.15	0.0860

Table 3.11 Calibration data of Zn by fixing loading flow rate at 3 ml min^{-1}, various loading times at different concentrations (continued)

μg ml^{-1} Zn	Loading time (min)	μg Zn	Peak height (Abs)
0.05	1.0	0.15	0.0860
0.05	1.0	0.15	0.0878
0.05	1.5	0.225	0.1290
0.05	2.0	0.30	0.1685
0.10	1.0	0.30	0.1648
0.10	1.0	0.30	0.1616
0.10	1.5	0.45	0.2312
0.10	2.0	0.60	0.2903
0.50	1.0	1.5	0.4301
0.50	1.5	2.25	0.4444
0.50	2.0	3.0	0.4731
1.0	1.0	3.0	0.4444
1.0	1.5	4.5	0.4731
1.0	2.0	6.0	0.4731

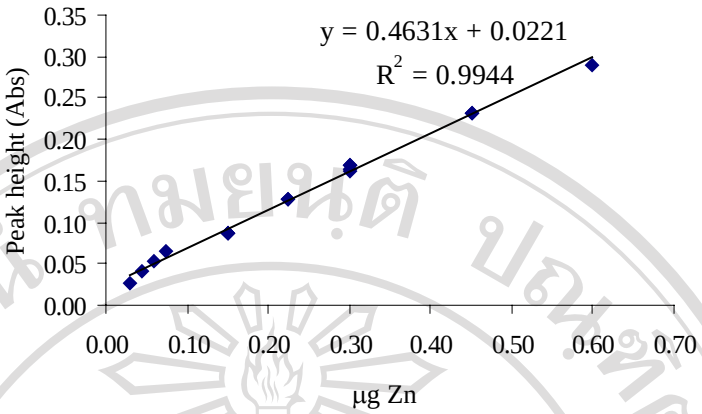

Figure 3.12 Calibration graph of Zn by various loading times at loading flow rate 3 ml min^{-1}

The single standard calibration was used in further experiments as shown in Tables 3.12-3.15 and Figures 3.13-3.16. Single standard calibration equations of Cd, Cu, Pb and Zn were obtained with the relationships: Cd; y=0.4243x+0.0047, Cu; y=0.0684x+0.0023, Pb; y=0.0208x+0.0017 and Zn; y=0.3461x+0.0344, when y is peak height and x is microgram of cations.

Table 3.12 Single standard calibration of Cd using 0.03 μg ml^{-1}Cd at loading time 20 to 120 seconds and constant flow rate 3 ml min^{-1}

μg ml^{-1} Cd	Loading time (sec)	μg Cd	Peak height (Abs)
0.03	20	0.030	0.0177
	30	0.045	0.0234
	60	0.090	0.0436
	90	0.135	0.0613
	120	0.180	0.0815

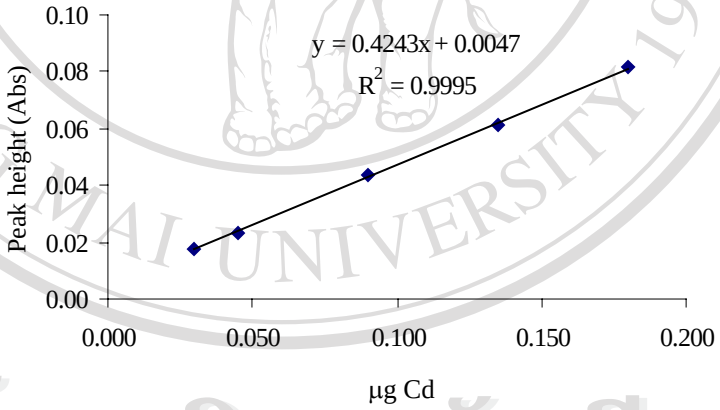

Figure 3.13 Single standard calibration of Cd

Table 3.13 Single standard calibration of Cu using 0.10 μg ml^{-1} Cu at loading time 0.5 to 3.0 minutes and constant flow rate 3 ml min^{-1}

μg ml^{-1} Cu	Loading time (min)	μg Cu	Peak height (Abs)
0.10	0.5	0.15	0.0123
	1.0	0.30	0.0229
	1.5	0.45	0.0335
	2.0	0.60	0.0436
	2.5	0.75	0.0536
	3.0	0.90	0.0637

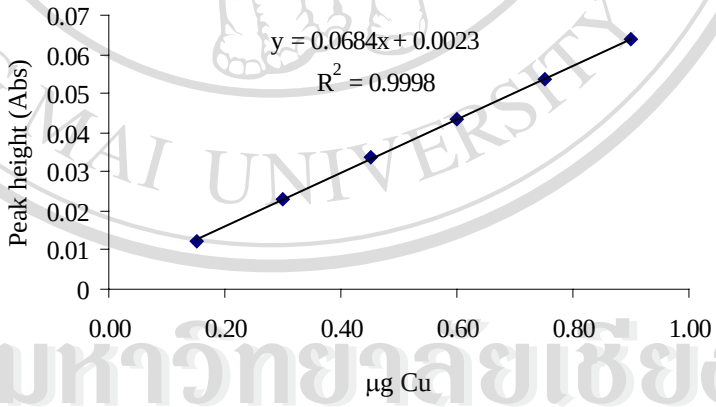

Figure 3.14 Single standard calibration of Cu

Table 3.14 Single standard calibration of Pb using 0.50 μg ml^{-1} Pb at loading time 10 to 70 seconds and constant flow rate 3 ml min^{-1}

μg ml^{-1} Pb	Loading time (sec)	μg Pb	Peak height (Abs)
0.50	10	0.25	0.0068
	20	0.50	0.0121
	30	0.75	0.0172
	40	1.00	0.0226
	50	1.25	0.0276
	60	1.50	0.0327
	70	1.75	0.0381

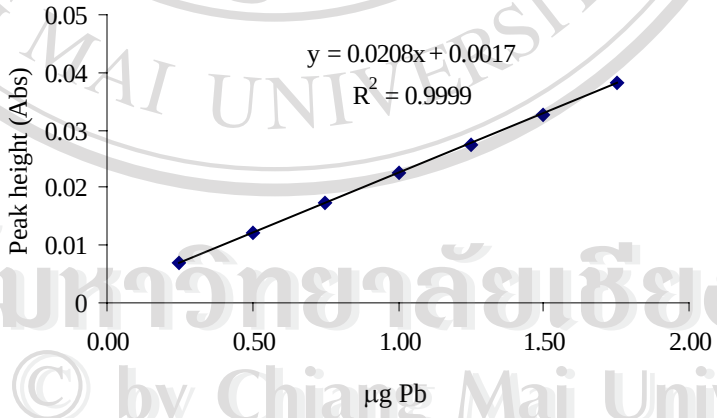

Figure 3.15 Single standard calibration of Pb

Table 3.15 Single standard calibration of Zn using 0.05 μg ml^{-1}Zn at loading time 1.0 to 3.0 minutes and constant flow rate 3 ml min^{-1}

μg ml^{-1} Zn	Loading time (min)	μg Zn	Peak height (Abs)
0.05	1.0	0.150	0.0835
	1.5	0.225	0.1149
	2.0	0.300	0.1395
	2.5	0.375	0.1655
	3.0	0.450	0.1880

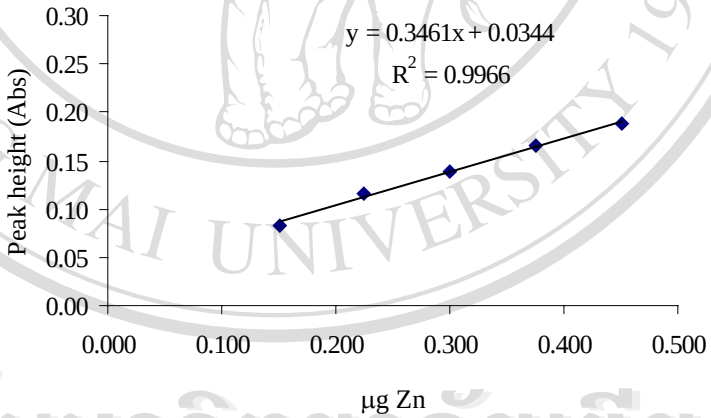

Figure 3.16 Single standard calibration of Zn

3.1.3 Recoveries study by using single standard calibration

Using the FI-FAAS manifold in Figure 2.2 with proposed conditions (1.0 M buffer solution (pH 5.4), loading flow rate 3 ml min^{-1} and eluent flow rate 5 ml min^{-1}), the recovered yields of cations were investigated for wastewater samples, both total cations and dissolved cations.

Water samples for total cation determinations were spiked with a mixture of standard cations (0.03 μg ml^{-1} Cd, 0.04 μg ml^{-1} Cu, 0.40 μg ml^{-1} Pb and 0.018 μg ml^{-1} Zn), as were water samples for dissolved cation determinations (0.04 μg ml^{-1} Cu, 0.40 μg ml^{-1} Pb and 0.013 μg ml^{-1} Zn). Water samples without standard cations and with spiked standard cations were loaded onto the on-line FI system, followed by determination of Cd, Cu, Pb and Zn using FAAS.

The microgram amounts of cations in wastewater samples were calculated by replacing the peak height for water samples in the calibration equation of the single standard calibration (μg = concentration x loading flow rate x loading time was used to calculate concentrations in water samples). The loading flow rate was kept constant at 3 ml min^{-1}, and the loading time depended on the concentration range for each water sample. The recovery for the proposed method was checked by adding the standard cations in water samples, in order to study the matrix effect during the preconcentration [84]. The results obtained are presented in Table 3.16 and Table 3.17. The recoveries of total cations and dissolved cations were found to be in the range 99-101%, showing that the matrixes of these samples had no remarkable effect on the preconcentration.

Table 3.16 Recoveries study for total cations

Cations	Water samples	Added ($\mu g\ l^{-1}$)	Found ($\mu g\ l^{-1}$)	Recovery* (%)
Cd	total cation	0	0 [b]	
	total cation	30	30.3 [c]	100.9
Cu	total cation	0	42.7 [b]	
	total cation	40	82.2 [c]	98.8
Pb	total cation	0	788.5 [b]	
	total cation	400	1187.5 [c]	99.8
Zn	total cation	0	17.6 [b]	
	total cation	18	35.4 [c]	98.9

* Recovery = ((c-b)/a) x 100 and 10 fold dilution for Pb and Zn

Table 3.17 Recoveries study for dissolved cations

Cations	Water samples	Added ($\mu g\ l^{-1}$)	Found ($\mu g\ l^{-1}$)	Recovery* (%)
Cu	dissolved cation	0	41.5 [b]	
	dissolved cation	40	81.7 [c]	100.5
Pb	dissolved cation	0	351.0 [b]	
	dissolved cation	400	756.4 [c]	101.4
Zn	dissolved cation	0	17.3 [b]	
	dissolved cation	13	30.3 [c]	100.0

* Recovery = ((c-b)/a) x 100 and 10 fold dilution for Pb and Zn

3.1.4 Application to water samples

The proposed method was applied to natural water and wastewater. After collection, the samples were digested (2.2.2.1) and the total cations were determined (2.4.1). For these experiments, the single standard calibration graphs were used. The results for cadmium, copper, lead and zinc are summarized in Table 3.18.

Table 3.18 Amount of cations in water samples

Water samples	Amounts of cations ($\mu g\ l^{-1}$)			
	Cd	Cu	Pb	Zn
Tap water	1.1	5.9	2.0	304
Surface water 1	1.7	2.6	3.3	918
Surface water 2	1.4	1.6	9.0	132
Surface water 3	2.1	1.3	7.0	49.3
Surface water 4	1.9	1.1	5.5	51.4
Surface water 5	1.8	2.7	7.5	73.7
Wastewater	1.8	42.7	7885	176

3.2 Flow injection in-valve mini-column pretreatment combined with ion chromatography for cadmium, lead and zinc determination

3.2.1 Optimization of ion chromatographic method

The conditions, mobile phase concentration, and flow rate of mobile phase for ion chromatographic separation were optimized. An organic acid eluent, a mixture of tartaric acid/oxalic acid, was used as the mobile phase since this organic acid eluent can separate Cd, Cu, Pb and Zn on the PBDMA stationary phase [20]. The separation and retention of cations on the PBDMA stationary phase is greatly influenced by various mobile phase concentrations.

Table 3.19 Concentrations of tartaric acid and oxalic acid

Concentration (mM)		Retention time (min)				Total analysis time (min)	Comments
Tartaric acid	Oxalic acid	Cu	Zn	Cd	Pb		
3.0	2.0	1.1	4.4	11.8	12.9	17	Bad resolution of Cd and Pb (Figure 3.17a)
1.5	2.0	1.1	5.2	15.4	15.4	20	Co-elution of Cd and Pb (Figure 3.17b)
3.0	1.5	1.4	6.5	17.0	20.5	25	Good resolution of all cations (Figure 3.17c)
3.0	1.0	1.9	9.4	23.0	31.3	35	Good resolution of all cations (Figure 3.17d)

Table 3.19 summarizes the study. Various concentrations of tartaric acid/oxalic acid in mixtures were investigated to achieve a good separation for some cations (Cd, Cu, Pb and Zn) with directly injected 20 µl of standard Cd, Cu, Pb and Zn mixture to a universal column, followed by conductivity detection. The retention time of cations of interest in the presence of a mobile phase followed the order Cu<Zn <Cd<Pb, and separation was achieved within 25 minutes for 3 mM tartaric acid/1.5 mM oxalic acid mixture (Figure 3.17c) and 35 minutes for 3 mM tartaric acid/1 mM oxalic acid mixture (Figure 3.17d). However, the use of two eluent ratios produces a good resolution between the peaks.

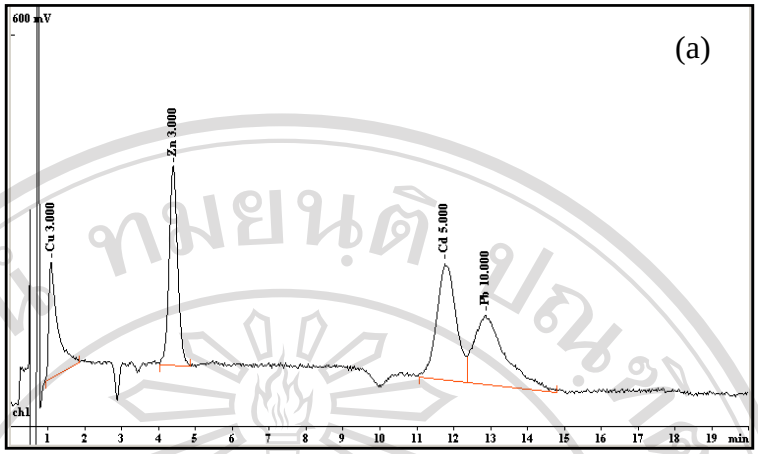

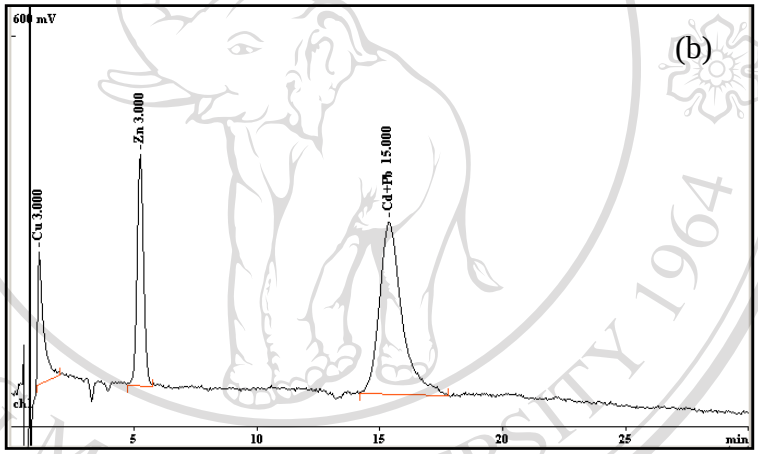

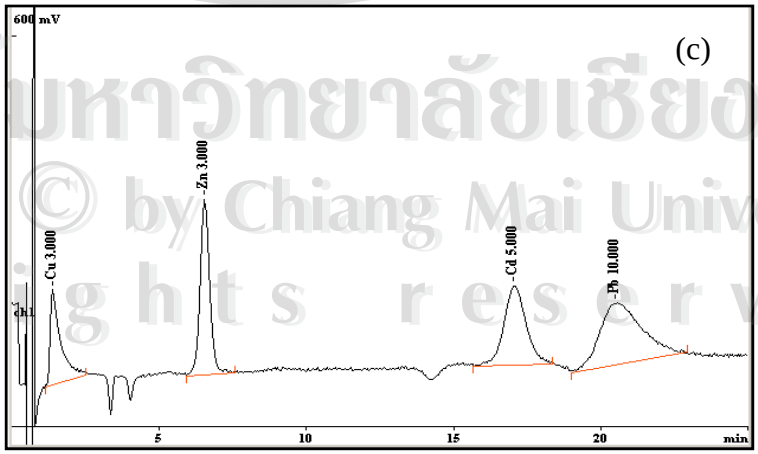

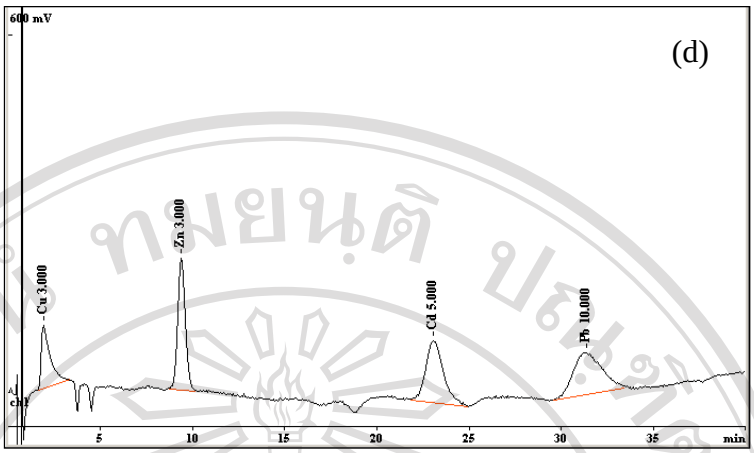

Figure 3.17 Chromatograms of cations in Milli-Q water at different concentration ratios of tartaric acid and oxalic acid as mobile phase; (a) 3 mM tartaric acid/2 mM oxalic acid, (b) 1.5 mM tartaric acid/2 mM oxalic acid, (c) 3 mM tartaric acid/1.5 mM oxalic acid and (d) 3 mM tartaric acid/1 mM oxalic acid

3.2.2 Combination of FI-IC system

The main aim of design of the FI-IC system (Figure 2.3) is to simplify and reduce operations of sample pretreatment, which leads to improvement of precision and reduction of interference in the sample matrix. This sample pretreatment method and coupling to an ion chromatograph was optimized for reagent compatibility.

3.2.2.1 Optimization of FI system with in-valve column (FI-IC)

Using the manifold in Figure 2.4 and optimal conditions of FI system in Table 3.20, the pH of eluate and the elapsed time, which is the elution time to move the analyte zone into the sample loop of the ion chromatograph (Figure 2.5), were studied.

Table 3.20 Proposed conditions for FI system with in-valve mini-column

Parameters	Conditions
buffer for adsorption process	1.0 M ammonium acetate buffer pH 5.4
loading flow rate	3 ml min^{-1}
eluent	2.0 M nitric acid
eluent flow rate	1.6 ml min^{-1}
buffer for eluate	sodium citrate buffer pH 3
base for neutralized eluate	2.0 M sodium hydroxide

The eluent of 2.0 M HNO_3 is very acidic and not suitable for injection into the ion chromatograph. It would affect the analytical column, and for a universal cation column, too low or too high pH solution must be avoided for the PBDMA stationary phase coated on silica. For a solution below pH 2, covalent bonds linking the ion exchange functionality become unstable and the functional groups are cleaved, while for a solution of pH over 8, the silica matrix may be dissolved [85]. The eluate acid solution from the FI system was then neutralized with 2.0 M NaOH and the pH controlled with sodium citrate buffer solution at pH 3 before flowing into

the sample loop and then being injected to the ion chromatograph. The results in Figure 3.18a show the chromatogram of a blank solution obtained on-line from the FI system to the ion chromatograph. A blank solution (without cations) was loaded on the in-valve mini-column and followed by the on-line elution process with 2.0 M HNO_3 for the FI operation. The baseline of the blank solution in the chromatogram exhibits a large, early elution peak, which is that of a high concentration of unretained Na^+ ion. Because the conductivity of Na^+ ion is lower than that of H^+ ion, a baseline drift occurs from change in the Na^+/H^+ ratio. In Figure 3.18b, the chromatogram of a mixture of cations (Cd, Cu, Pb and Zn) was obtained by using the same conditions as for the blank. From the chromatogram, the conductivity of the unretained Na^+ ion causes a large peak and interferes with the Cu peak (t_R = 1.4 min) in the time range 0-5 minutes. Moreover, baseline drift occurred at the same peak position as the Pb peak. This could be solved by changing the mobile phase ratio to move the analyte peaks, as shown in Figure 3.18c and Figure 3.18d. Reducing oxalic acid's concentration from 1.5 mM to 1.0 mM increased the retention times of cations. This would be special for Pb with the smallest log K value (log K of Zn(II), Cd(II) and Pb (II) for oxalic acid= 4.9, 3.9 and 3.3, respectively).

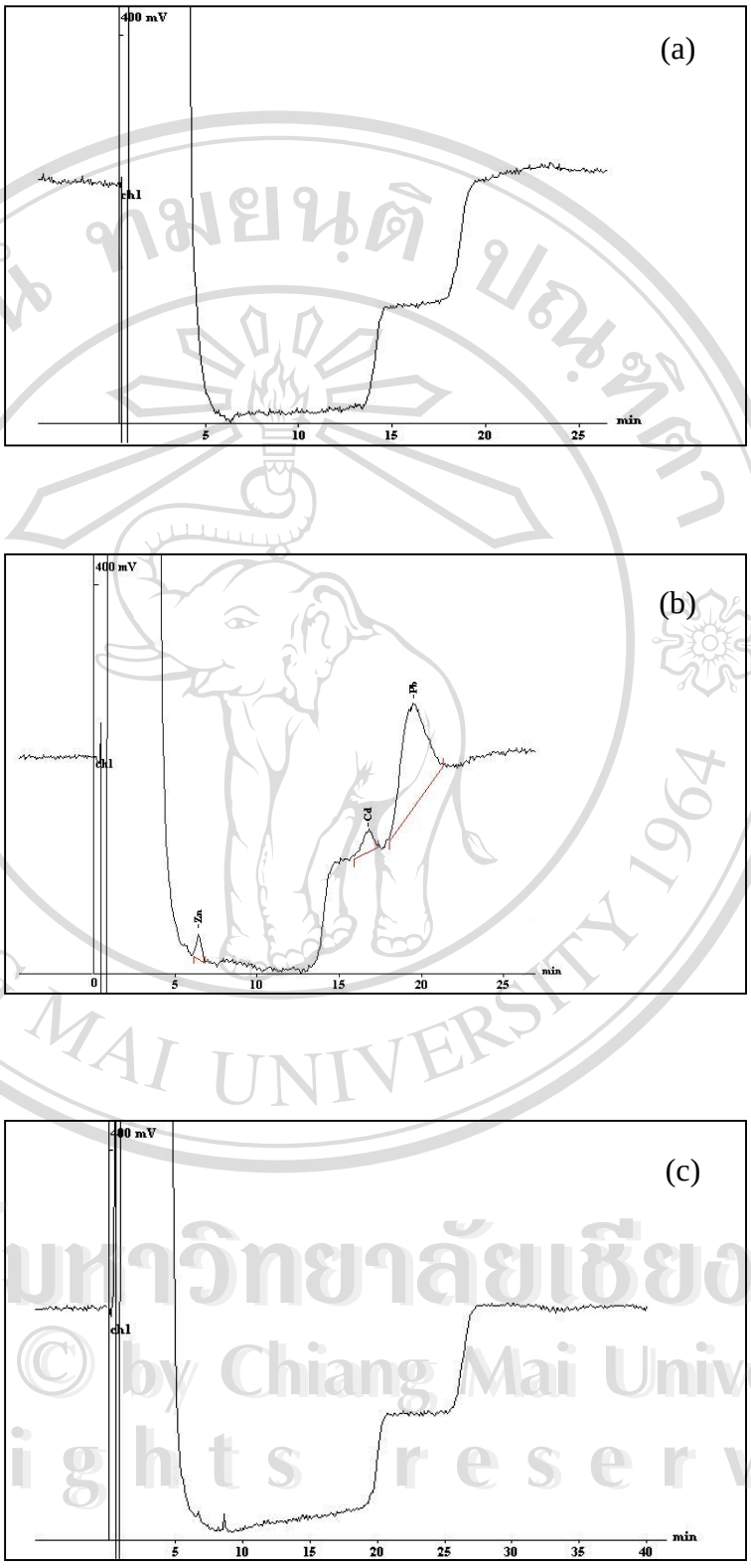

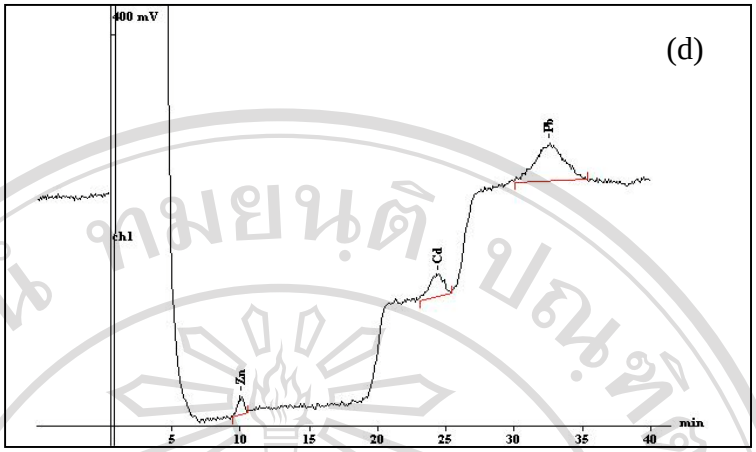

Figure 3.18 Chromatograms of blank solution without cations and cations (Cd=5 mg l^{-1}, Pb=10 mg l^{-1} and Zn=3 mg l^{-1}) by using the FI on-line sample pretreatment with loading time 1 min and loading flow rate 3 ml min^{-1} before injecting into ion chromatograph with elapsed time 24 seconds; (a) blank solution using 3 mM tartaric acid/1.5 mM oxalic acid as a mobile phase, (b) cations (Cd: t_R=16.7 min, Pb: t_R=19.3 min and Zn: t_R=6.4 min) using 3 mM tartaric acid/1.5 mM oxalic acid as a mobile phase, (c) blank solution using 3 mM tartaric acid/1 mM oxalic acid as a mobile phase, (d) cations (Cd: t_R=24.3 min, Pb: t_R=35.6 min and Zn: t_R=9.9 min) using 3 mM tartaric acid/1 mM oxalic acid as a mobile phase

The time to move the elution zone with high concentration of analytes from the FI system to the injection loop of the ion chromatograph is called elapsed time as depicted in Figure 2.5. When the FI valve was switched to the injection position and the time passed 24 seconds, then the IC valve was switched to

the injection position. The elapsed time affected the sensitivity of the proposed method. From the results, an elapsed time of 24 seconds was chosen for further work because it gave a higher sensitivity as shown in Table 3.21.

Table 3.21 Effect of elapsed time

Elapsed time	Retention time (min)			Peak area (millivolt)		
(sec)	Zn	Cd	Pb	Zn	Cd	Pb
20	11.87	26.32	-	2613	3313	-
24	11.62	26.13	34.09	5762	9015	8175
28	10.98	25.95	33.91	3971	5668	4392

3.2.2.2 Performance of the proposed method

Reproducibility tests were carried out for estimating the relative standard deviation (RSD) of the chromatographic peak areas. This data was obtained from five repeated injections at a loading time of 40 seconds for a concentration of 1 μg ml^{-1} of all interested cations. Average RSD values of 3.1%, 3.5% and 5.1% for Zn, Cd and Pb, respectively, were obtained (Table 3.22).

Table 3.22 Precision of method using 1 μg ml^{-1} with 40 seconds loading time (a flow rate of 3 ml min^{-1}) yielding 36 μg (5 replicates)

Cations	Peak area (millivolt)	%RSD
Zn	2729, 2803, 2878, 2766, 2942	3.1
Cd	4185, 4210, 4408, 3998, 4187	3.5
Pb	5174, 4752, 5192, 4816, 4651	5.1

Calibration was studied by collecting fractions of the eluate from the FI system to make a total volume of 3 ml. The solution was then injected into an IC. Table 3.23 summarizes data in the study with a flow rate of 3 ml min^{-1} for loading the standard solution into the FI column. Linear calibration graphs could be obtained, as in Figure 3.19. When calculating the micrograms of cation loaded on to the column from concentration (μg ml^{-1}) x loading flow rate (ml min^{-1}) x loading time (min), the microgram amounts are also shown in the Table 3.23. Plotting the peak area (y-axis) versus microgram (x-axis), a linear relation can be obtained, as reported in Figure 3.20.

Table 3.23 Data for calibration study

Cations	Original concentration ($\mu g\ ml^{-1}$)	Loading time (min)	μg of cation[a]	Final concentration of the 3 ml eluate solution ($\mu g\ ml^{-1}$)*	Peak area (millivolt)
Zn	0.5	2	3.0	1.0	584
	0.3	5	4.5	1.5	644
	0.5	3	4.5	1.5	683
	0.5	4	6.0	2.0	877
	0.3	10	9.0	3.0	1119
	0.5	6	9.0	3.0	1187
	0.3	15	13.5	4.5	1571
	1.0	2	6.0	2.0	611
	0.4	3	9.0	3.0	854
Cd	1.0	4	12.0	4.0	1128
	0.4	15	18.0	6.0	1579
	1.0	6	18.0	6.0	1808
	2.0	2	12.0	4.0	2875
	0.8	5	12.0	4.0	2835
	2.0	3	18.0	6.0	3614
Pb	2.0	4	24.0	8.0	4213
	0.8	10	24.0	8.0	4234
	0.8	15	36.0	12.0	5249
	2.0	6	36.0	12.0	5077

* = a/3

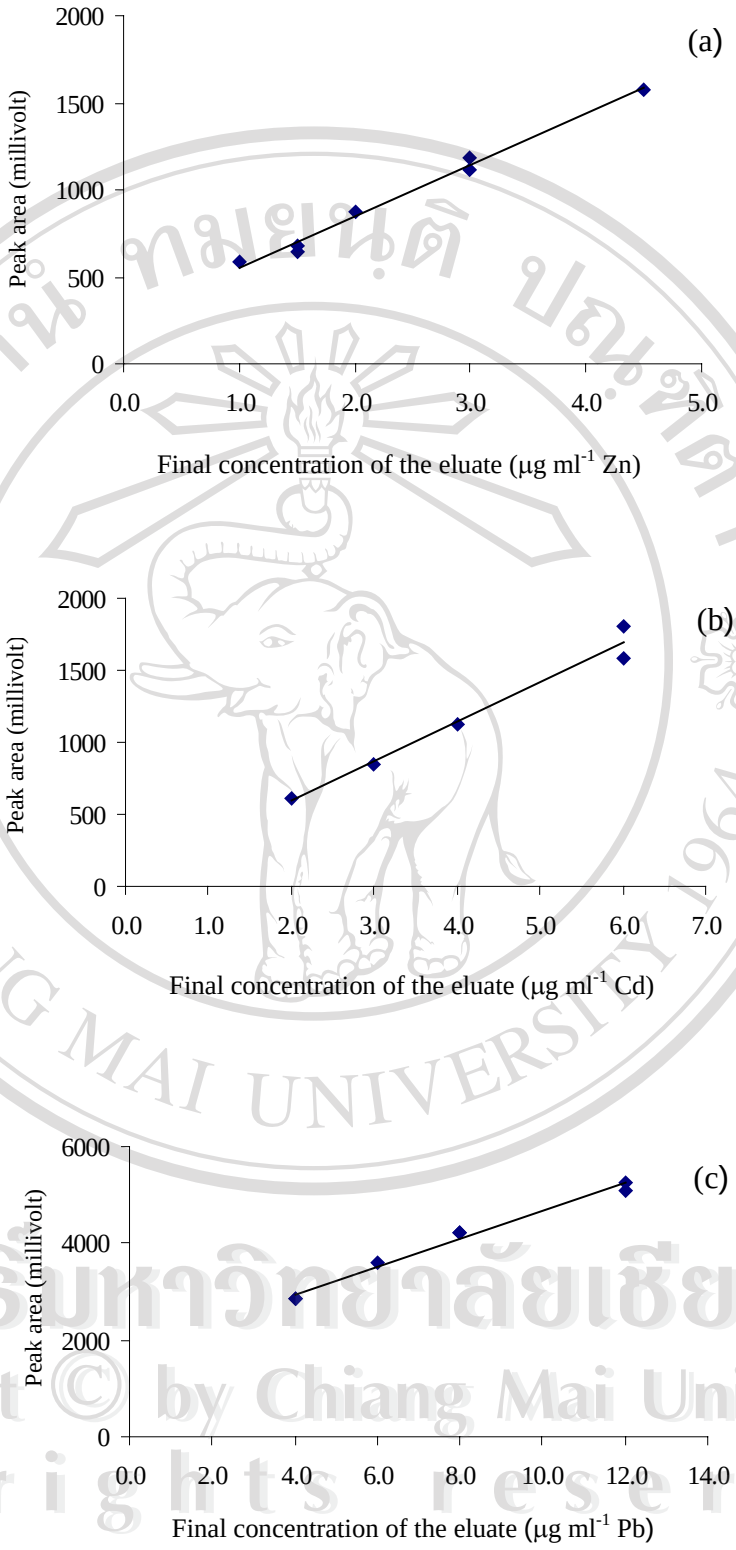

Figure 3.19 Calibration graphs obtained by using the data from Table 3.23 (a) Zn, (b) Cd and (c) Pb

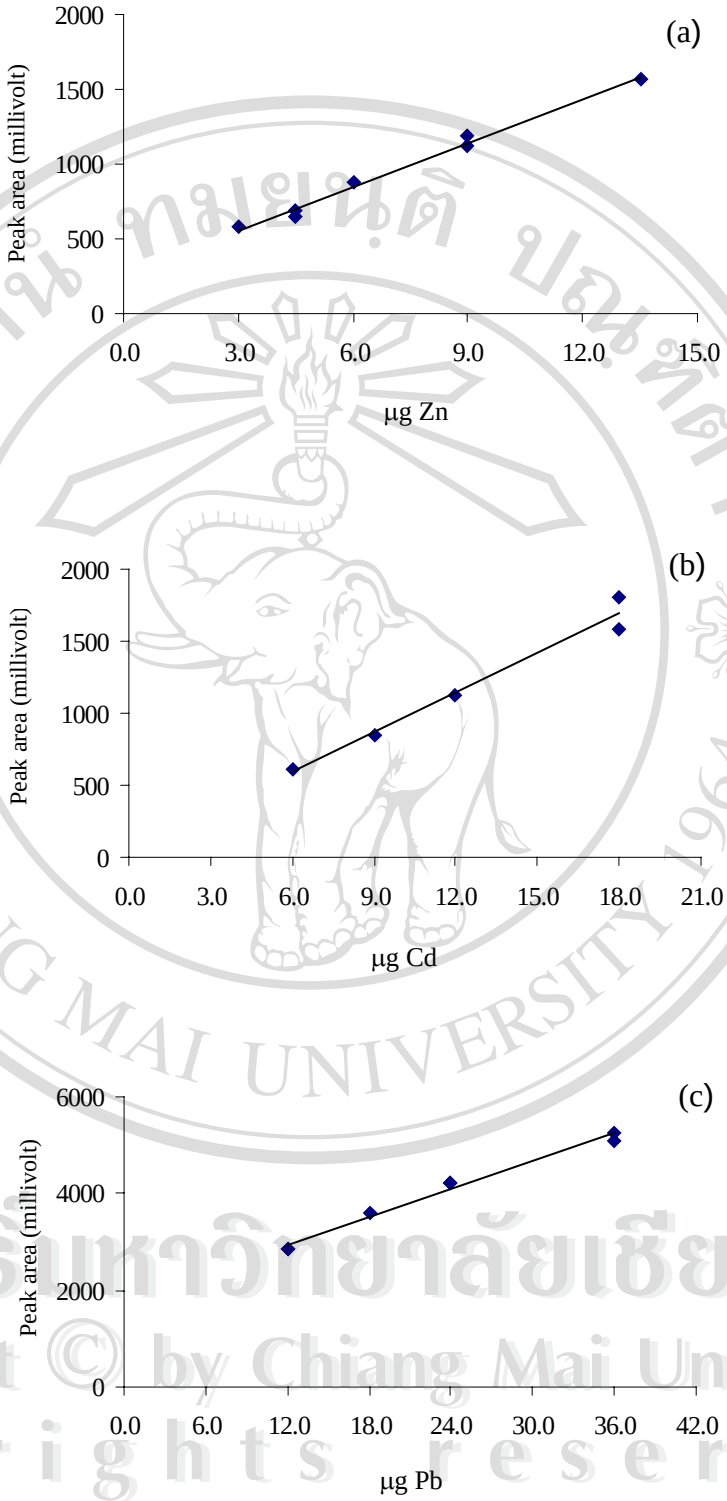

Figure 3.20 Conventional calibration graphs (a) Zn, (b) Cd and (c) Pb

From the study, it can be concluded that a single standard calibration could be constructed by using only one solution. Single standard calibration can be then be obtained by using a plot of peak area (y-axis) and micrograms of cation loaded (x-axis), which were obtained by loading only one standard solution of cation to the in-valve column with various loading times. The micrograms of cation was calculated by concentration (μg ml^{-1}) x loading flow rate (ml min^{-1}) x loading time (min). The plots were found to be linear. The peak area obtained depends on both the cation concentration and loading time. Table 3.24 represented the expression of single standard calibration of Zn, Cd and Pb and corresponding ranges of micrograms of cation.

Table 3.24 Single standard calibration expressions

Cations	Equation	Range (μg)	r^2
Zn	y=89x-553	60-200	0.9860
	y=59x+5561	200-600	0.9916
Cd	y=105x-99	6-25	0.9892
	y=44x+1035	25-60	0.9810
Pb	y=93x+762	18-54	0.9825
	y=43x+3559	54-180	0.9917

The accuracy of the proposed method was checked by determination of cation mixtures in zinc ore samples and zinc ore samples with spiked

standard cations. The recoveries of Cd, Zn and Pb were calculated as shown in Table 3.25.

Table 3.25 Recoveries of cations

Cations	Sample	Added ($\mu g\ ml^{-1}$)	Found ($\mu g\ ml^{-1}$)	Recovery* (%)
Zn	zinc ore sample	0.0	210.6 [b]	99
	zinc ore sample	100.0 [a]	309.9 [c]	
Cd	zinc ore sample	0.0	1.1 [b]	95
	zinc ore sample	1.5 [a]	2.6 [c]	
Pb	zinc ore sample	0.0	41.8 [b]	105
	zinc ore sample	40.0 [a]	83.9 [c]	

* Recovery = ((c-b)/a) x 100

3.2.2.3 Analysis of zinc ore samples

To determine Zn, Cd and Pb in zinc ore samples having high amounts of interference components, the samples were digested with nitric acid. A digested sample solution was on-line pretreated by the ion exchange column in the FI system and continuously analyzed with ion chromatography. The results obtained agree with reference methods (ICP-AES and AAS) as shown in Table 3.26.

Table 3.26 Analysis of zinc ore samples

Sample	Concentration found (%)								
	Zn			Cd			Pb		
	FI-IC[a]	ICP-AES[b]	AAS[b]	FI-IC[a]	ICP-AES[b]	AAS[b]	FI-IC[a]	ICP-AES[b]	AAS[b]
A	25.3±0.6	30.4±0.2	30.4±0.2	0.27±0.01	0.33±0.02	0.32±0.02	6.0±0.2	5.8±0.3	5.7±0.3
B	49.5±1.2	45.1±0.5	45.1±0.5	0.19±0.01	0.20±0.02	0.20±0.02	5.4±0.2	6.3±0.3	6.3±0.3
C	42.4±0.8	45.1±0.5	45.1±0.5	0.20±0.01	0.20±0.02	0.19±0.02	4.4±0.2	6.3±0.3	6.3±0.3
D	26.9±0.4	27.8±0.2	27.8±0.3	0.18±0.01	0.19±0.02	0.19±0.02	4.6±0.1	4.8±0.3	4.8±0.3
E	28.5±0.4	27.9±0.3	27.8±0.3	0.18±0.01	0.19±0.02	0.18±0.02	4.6±0.2	4.8±0.3	4.8±0.3

[a] The proposed method

[b] Analyzed by the Mineral Resources Region 3 (Chiang Mai)

Both (a) and (b) were from triplicate results: mean±standard deviation

3.3 On-line preconcentration and quantitation of benzene, toluene and *p*-xylene by using Raman liquid-core waveguide sensor

3.3.1 Raman spectra of benzene, toluene and *p*-xylene

A three dimensional plot of raw Raman data collected during the elution of benzene, toluene and *p*-xylene is shown in Figure 3.21a. A mixture of an aqueous solution containing 70 mg l^{-1} benzene, 100 mg l^{-1} toluene and 100 mg l^{-1} *p*-xylene in 1000 µl was initially preconcentrated into the waveguide. In the extraction and elution step, a 30 µl volume of acetonitrile in water was used to extract the analytes from the waveguide. The spectra show both the Raman response and the kinetic desorption information of the extracted and eluted analytes. The waveguide does not permit water to adsorb significantly onto its surface and is chemically resistant to most other solvents. Moreover, it has low solubility in selected perfluorinated solvents, on the order of 3-15%. The waveguide does permit the non-polar analytes to absorb into the inner wall of the waveguide, in the sub-micron thickness range [64], possibly by way of the nanoporous Teflon-AF 2400 structure, and so benzene, toluene and *p*-xylene can readily be extracted and preconcentrated from aqueous solution into the waveguide inner wall. Acetonitrile was chosen as the organic component of the eluting solvent because it provided a Raman shift different from the Raman peaks of the analytes. It was shown that the elution strength of 70% acetonitrile in 30% water was optimal for extraction, since the analytes quantitatively eluted from the waveguide. Acetonitrile and the analytes, benzene, toluene and *p*-xylene, have sufficiently similar organic character and so the analytes prefer to elute from the

waveguide rather than be retained on it [86]. Another reason acetonitrile was used is that it did not degas at the laser wavelength or power being used to perform the Raman analysis. Figure 3.21b shows the two-dimensional plot of the same data as in Figure 3.21a. The spectra were obtained during the extraction/elution phase of the experiment. A total of 40 spectra were taken during 10 minutes of elution. The acquisition time for each spectrum was 15 seconds (5 exposures and 3 accumulations). The analyte signals are more clearly seen in Figure 3.21b. The Raman frequencies of the aromatic ring breathing modes of benzene and toluene occur at 992 $cm^{-1}$and 1004 cm^{-1}, respectively. The Raman peak of *p*-xylene at 1206 cm^{-1} was indicative of the C-C ring [87]. Acetonitrile bands are very intense due to the high concentration in the waveguide during the elution step; therefore, it was necessary to perform background subtraction and correction for better data analysis and clarity.

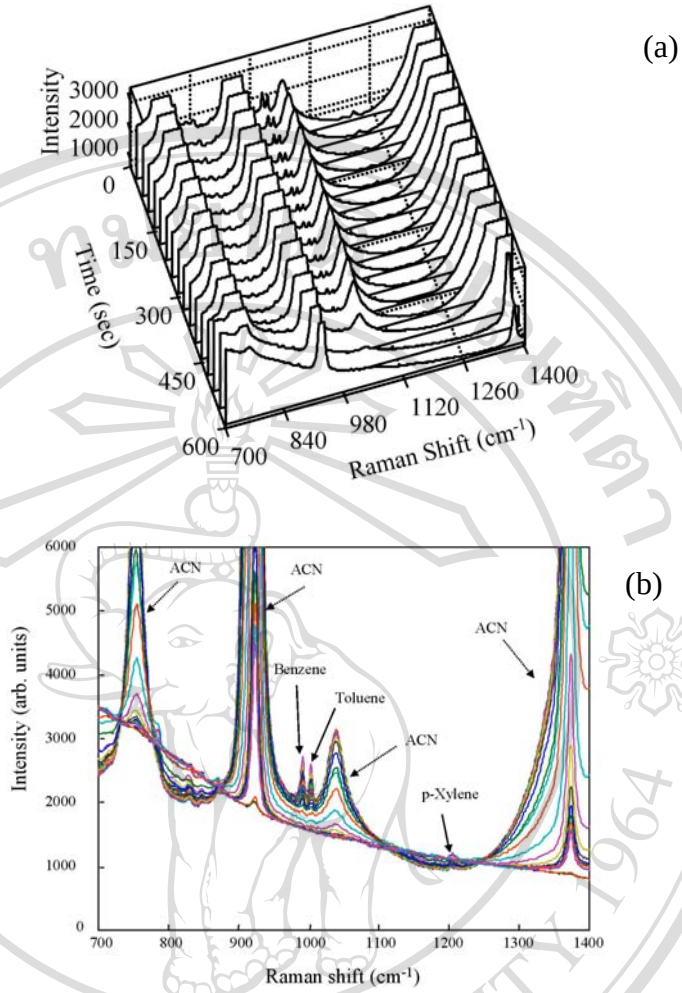

Figure 3.21 (a) Three-dimensional plot of raw Raman signal during the extraction of a 70 mg l^{-1} benzene, 100 mg l^{-1} toluene and 100 mg l^{-1} *p*-xylene mixture. The plot was enlarged on the intensity axis to 3000 arb. units to cut some high intensity of acetonitrile and focus on analytes peak. Every other spectrum was omitted for clarity.

(b) Two-dimensional plot of this data on the Raman shift axis. The large Raman bands for acetonitrile (ACN) are also labeled. Each signal trace was obtained during the time-dependent elution of the preconcentrated sample from the waveguide.

3.3.2 Background-subtracted Raman spectra

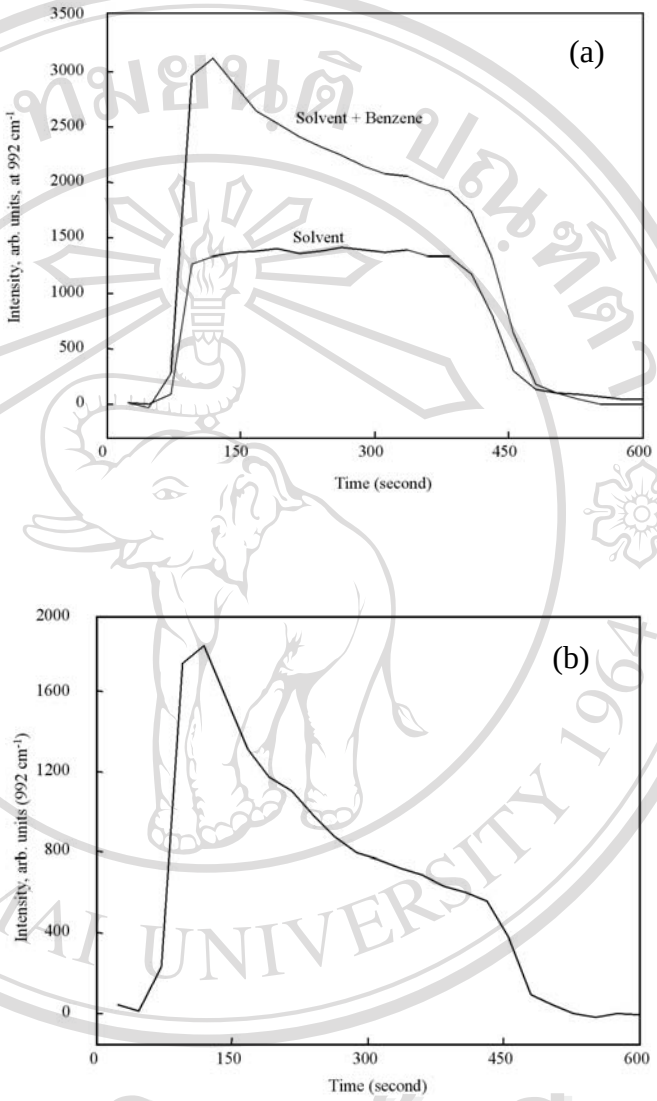

Figure 3.22 (a) Elution time profile of extraction solvent only (70% acetonitrile/30% water) and the extraction of 75 mg l^{-1} benzene (as single analyte in sample). These profiles contain the summation of signals of 992 cm^{-1}, which is the maximum sensitivity for benzene.

(b) The elution time profile of benzene after background correction

Figure 3.22a shows the elution time profiles of a 75 mg l^{-1} benzene sample initially preconcentrated, obtained from the analyte extraction/elution step, along with the baseline collection step (background signal). Both elution time profiles were processed at the maximum signal of benzene corresponding to a Raman shift at 992 cm^{-1}. Figure 3.22b shows the elution time profile of benzene, following baseline subtraction. The figure shows that benzene can be quantitatively extracted from the waveguide tubing walls within 8 minutes. In this figure the temporal information is still apparent. In the final algorithm the temporal information is eliminated for clarity by summing the baseline-corrected response at each wavenumber and then plotting the resulting Raman spectra as a function of wavenumber only.

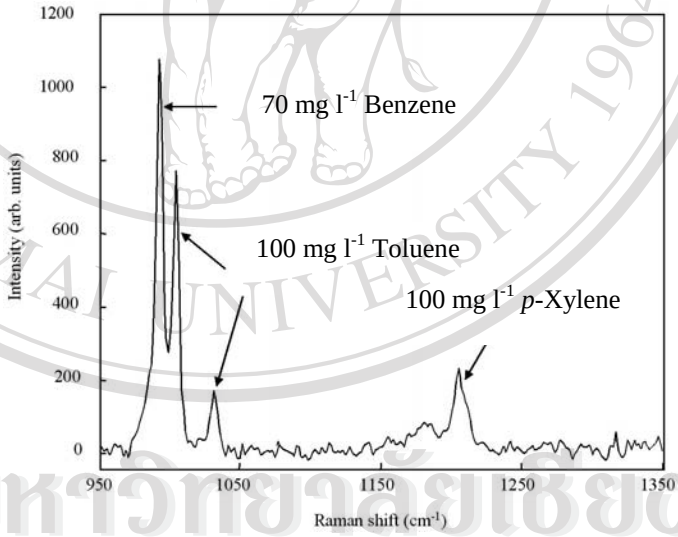

Figure 3.23 Background-subtracted Raman spectrum of mixture containing 70 mg l^{-1} benzene, 100 mg l^{-1} toluene and 100 mg l^{-1} *p*-xylene using the data presented in Figure 3.21. The data have also been summed at each time interval, thus eliminating the time axis.

The results shown in Figure 3.23 illustrate the Raman spectrum of the analyte mixture shown previously in Figure 3.21 after application of the background correction procedure. The procedure removed the acetonitrile signal contribution as well as reduced the data density by eliminating the time dependence. In the first step of background correction, the two-dimensional matrices of sample data and background data are reduced to vectors of background data and sample data along the spectra axis. This is completed by averaging the signal during the elution of the sample plug. A first-order polynomial fit of the background vector to the sample vector was then subtracted from the sample vector. The polynomial fit accounts for small fluctuations in the baseline and laser intensity. The benefits of the acetonitrile background subtraction and correction routine are evident in the appearance of the 1031 cm^{-1} Raman peak of toluene peak that can be easily resolved from the background. The background-corrected spectrum shows very good selectivity and overall sensitivity for benzene, toluene and *p*-xylene.

3.3.3 Calibration graph

Calibration data were obtained from Raman signals of individually run analytes, which after baseline correction are between 975 cm^{-1} and 1005 cm^{-1} Raman shift for benzene and between 985 cm^{-1} and 1015 cm^{-1} Raman shift for toluene. The peak signals at 992 cm^{-1} for benzene and at 1004 cm^{-1} for toluene were used for calibration, as shown in Figure 3.24a and Figure 3.24b, respectively. The calibration plot for benzene and toluene were constructed using the peak areas from the signal calibration data. Calibration graphs for a concentration range from 10 mg l^{-1} to

75 mg l^{-1} are shown in Figure 3.25. The correlation coefficients of linear regression analysis were 0.9814 for benzene and 0.9977 for toluene. The relative standard deviation obtained in this analysis was 3.0% for three replicate measurements at 50 mg l^{-1} benzene. The waveguide material was not extensively studied above 75 mg l^{-1} as demonstrated in Figure 3.25, since above 75 mg l^{-1} the same apparatus could be applied for the analysis without requiring explore the upper concentration limit up to the point of saturation during preconcentration.

For *p*-xylene, calibration data and calibration graph are not depicted here but they could be obtained as benzene and toluene.

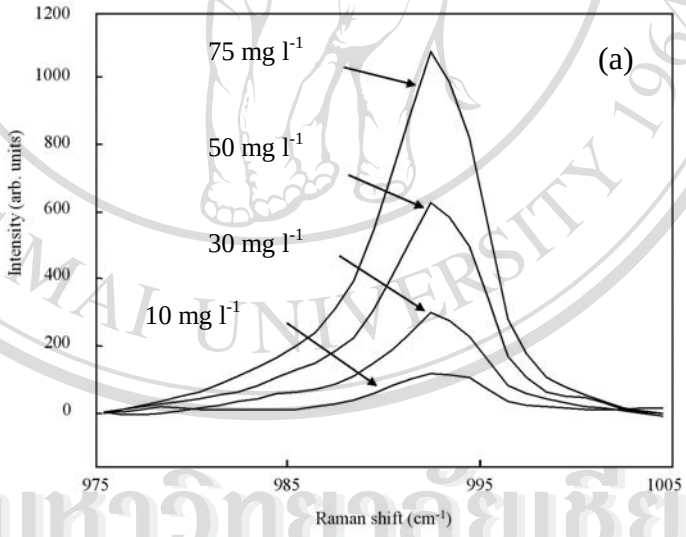

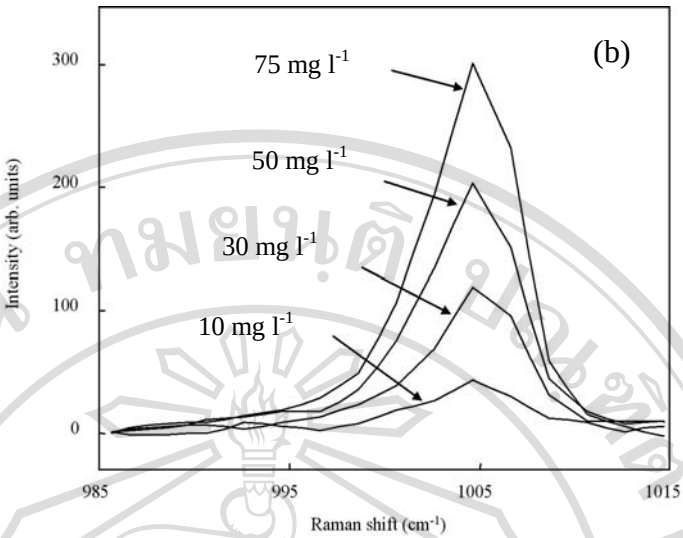

Figure 3.24 Raman spectra of samples over a concentration range 10-75 mg l^{-1} of (a) benzene and (b) toluene, following the background correction procedure. Samples were initially preconcentrated in water and then eluted in 70% acetonitrile/30% water.

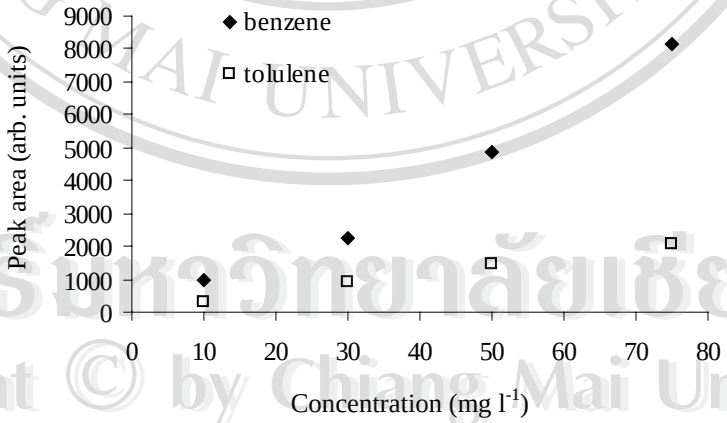

Figure 3.25 Calibration graphs are shown in the intensity of the Raman signal plotted versus the concentration of benzene and toluene. Samples were initially preconcentrated in water and then eluted in 70% acetonitrile/30% water.

3.3.4 Limit of detection

The limit of detection (LOD) was calculated from the peak height of the 10 mg l^{-1} benzene signal and representative baseline noise.

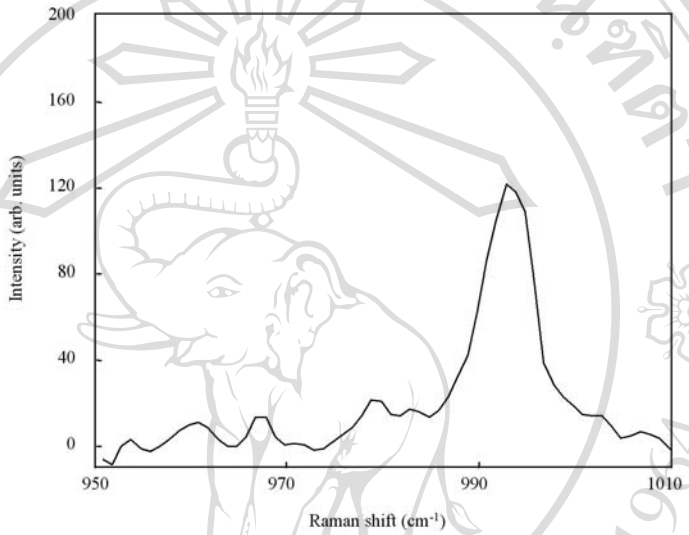

Figure 3.26 Raman spectra of a 10 mg l^{-1} benzene sample and representative baseline noise. The limit of detection of the method was 730 μg l^{-1} for benzene.

Figure 3.26 shows for typical data used for LOD calculation. The LOD was determined to be 730 μg l^{-1} for benzene. Note that LOD is a figure-of-merit and at LOD the signal would just begin to be discernable from the baseline noise (3σ) [88]. LOD for benzene with the same waveguide system but without using the preconcentration procedure was determined to be 10 mg l^{-1}. Thus, a factor of 14 enhancement in LOD is provided by the preconcentration procedure with the enhancement factor for benzene calculated as LOD without preconcentration divided by LOD using preconcentration. This experimental enhancement is in reasonable

agreement with the theoretical enhancement of 33 calculated by taking the ratio of the sample volume (1000 μl) divided by the elution volume (30 μl). The agreement is reasonable given the noise in the baseline does not proportionately relate to the analyte signal during the data reduction procedure applied with the preconcentration procedure. The experimental LOD obtained using the preconcentration procedure is quite satisfactory for many applications.

For LOD of toluene and *p*-xylene were not reported. However, the method to calculate LOD of toluene and *p*-xylene are the same as for benzene.